Thermodynamic Properties of the Kinesin Neck-Region Docking to the Catalytic Core

S. Rice, Y. Cui, C. Sindelar, N. Naber, M. Matuska, R. Vale, and R. Cooke

Department of Cellular and Molecular Pharmacology, University of California, San Francisco, California 94143

ABSTRACT   Kinesin motors move on microtubules by a mechanism that involves a large, ATP-triggered conformational change in which a mechanical element called the neck linker docks onto the catalytic core, making contacts with the core throughout its length. Here, we investigate the thermodynamic properties of this conformational change using electron paramagnetic resonance (EPR) spectroscopy. We placed spin probes at several locations on the human kinesin neck linker and recorded EPR spectra in the presence of microtubules and either 5′-adenylylimidodiphosphate (AMPPNP) or ADP at temperatures of 4–30°C. The free-energy change (ΔG) associated with AMPPNP-induced docking of the neck linker onto the catalytic core is favorable but small, about 3 kJ/mol. In contrast, the favorable enthalpy change (ΔH) and unfavorable entropy change ($T\Delta S$) are quite large, about 50 kJ/mol. A mutation in the neck linker, V331A/N332A, results in an unfavorable ΔG for AMPPNP-induced zipping of the neck linker onto the core and causes motility defects. These results suggest that the kinesin neck linker folds onto the core from a more unstructured state, thereby paying a large entropic cost and gaining a large amount of enthalpy.

INTRODUCTION

Kinesin motors use the energy of ATP hydrolysis to drive unidirectional motion along microtubules, powering a variety of motile processes in cells (Vale and Milligan, 2000). All kinesins have a homologous ~330 amino acid catalytic core that binds ATP and microtubules. Immediately adjacent to the catalytic core is the neck linker, a ~15 amino acid segment which has been shown to be critical for force generation and directionality (Case et al., 1997, 2000; Henningsen and Schliwa, 1997; Rice et al., 1999; Rosenfeld et al., 2001). Kinesin dimers move processively, undergoing several enzymatic cycles and coupled mechanical steps before releasing from the microtubule. To accomplish this, the two heads of a kinesin dimer coordinate their ATPase cycles (Gilbert et al., 1998; Hackney, 1994; Ma and Taylor, 1997a).

Kinesin dimers are able to move processively forward on microtubules for hundreds of steps, taking only ~5–10% backward steps (Schnitzer et al., 2000; Vale et al., 1996). While walking processively forward, a single kinesin dimer consumes exactly 1 ATP per 8-nm step (Hua et al., 1997; Schnitzer and Block 1997) and moves under loads of up to 6 pN (Svoboda and Block, 1994; Visscher et al., 1999). As it can generate 48 pN·nm of work per step at high loads, kinesin is up to 50% efficient in converting the energy of ATP hydrolysis into forward mechanical work on the microtubule.

High-resolution electron-microscopy studies (Hoenger et al., 1998; Hoenger et al., 2000; Kikkawa et al., 2001) as well as x-ray crystal structures of the kinesin molecule (Kikkawa et al., 2001; Kozielski et al., 1997; Kull et al., 1996; Song et al., 2001; Yun et al., 2001) have yielded detailed structural information about the conformational

transitions that drive kinesin's motility. The ATP-driven conformational changes in the kinesin core are strikingly similar to those that occur in the myosin motors as well as G proteins (Kull and Endow, 2002). Nucleotide changes trigger the formation or breaking of salt bridges between the γ-phosphate of ATP and the N-terminal end of a highly conserved loop in the kinesin core called switch II. At the opposite end of switch II is the $\alpha 4$ helix, which acts as a mechanical relay of the nucleotide change to the neck linker/catalytic core interface. In the ADP- or nucleotide-free state, the $\alpha 4$ helix swings outward and downward, pushing the neck linker away from the catalytic core. In the ATP state, the $\alpha 4$ helix is brought closer to the nucleotide pocket, revealing contacts for neck-linker residues along the catalytic core (Sablin and Fletterick, 2001; Vale and Milligan, 2000). Thus, switch II and the $\alpha 4$ helix act as relays that change the neck-core interface, allowing the neck linker to dock to the core in triphosphate states and preventing docking in the ADP- or nucleotide-free state.

Schnitzer et al., (2000) have presented a detailed thermodynamic model for kinesin's highly efficient motility. By modeling molecular force clamp data recorded at several loads and ATP concentrations, they hypothesized that a load-dependent isomerization step occurs after ATP binding. Although it remains to be proven, this ATP-dependent isomerization step may be the ATP-induced docking of the neck linker to the enzymatic core that is described in other experiments (Rice et al., 1999; Rosenfeld et al., 2001). Kinesin motors may follow this highly efficient ATP-dependent isomerization (small free energy (ΔG)) with tight binding to the microtubule (large ΔG) to move efficiently against high loads. Although this is an attractive and feasible hypothesis, the changes in free energy that are associated with these conformational transitions have never been directly measured.

EPR spectroscopy has been shown to be a sensitive reporter of conformational changes both in the human kinesin neck linker (Rice et al., 1999) and in the kinesin family member

nonclaret disjunctional (NCD; Naber et al., 1997) motor, as well as in the myosin motors (Thomas and Cooke, 1980). EPR spectra with two or more components corresponding to different protein conformations immediately reveal the changes in ΔG between those conformations. By varying the temperature of the sample and collecting EPR spectra, one can determine the changes in enthalpy (ΔH) and entropy ($T\Delta S$) for a protein conformational change. In this work, we use EPR spectra of probes that are located along the kinesin neck linker to measure the ΔG and ΔH associated with transitions between different conformations of the kinesin neck linker. We find that the ΔG for the AMPPNP-induced docking of the neck linker onto the core is favorable but small. The magnitudes of the favorable ΔH and the unfavorable $T\Delta S$ for this conformational change are both very large, which is consistent with a transition from an unstructured neck-linker state to one that folds along the catalytic core. A mutation disrupting some contacts in the neck-linker–catalytic core interface (V331A/N332A) eliminates the favorable ΔG for AMPPNP-induced docking of the neck linker onto the core and exhibits motility defects. Collectively, our results suggest that the neck linker folds onto the catalytic core from an unstructured state. In doing so, it pays a high entropic cost, which is balanced out by a highly favorable gain in enthalpy. A model in which both the unstructured and folded neck-linker states play a role in the processive motility of kinesin is presented.

METHODS

Cloning, expression, and purification of kinesins used in this study

The cysteine-light (cys-light) kinesin proteins used in this study were cloned and purified as previously described (Rice et al., 1999). The V331A/N332A construct described in this study was prepared using Quikchange mutagenesis (Stratagene, La Jolla, CA) in either the cys-light K349 + C333 monomer or the cys-light K560 dimer construct and was confirmed by DNA sequencing. All proteins were expressed and purified as previously described (Rice et al., 1999).

Labeling with spin probes

A single cysteine-containing kinesin (C328, C330, or C333) in EPR-labeling buffer (25 mM piperazine-N, N',-bis(2-ethanesulfonic acid) (PIPES; pH 7), 50 mM NaCl, 2 mM MgCl$_2$, 1 mM EGTA, and 10 μM ATP) was incubated with 4-maleimido-2, 2, 6, 6-tetramethyl-1-piperidinoxy (MSL; Sigma Chemical Co.) overnight at 4°C. Excess spin label was removed by repeated concentration and dilution of the protein in a 3000-molecular weight cutoff centricon (Millipore, Bedford, MA). The labeling stoichiometry was determined by measuring protein concentration (Bradford assay with bovine serum albumin standards) and probe concentration by comparing labeled protein to known concentrations of spin label (Naber et al., 1997).

Activity of labeled constructs

Steady-state, microtubule-stimulated ATPase rates for wild-type and V331A/N332A mutant kinesins were measured using a coupled enzymatic assay (Woehlke et al., 1997). Tubulin preparation for all assays was performed as previously described (Woehlke et al., 1997). All constructs had

reasonable values of k_{cat} and K_m(MT) for microtubule-stimulated ATPase activity, which are summarized in Table 1.

EPR spectroscopy

EPR measurements were performed with an ER/200D EPR spectrometer from IBM Instruments, Inc. (Danbury, CT). First-derivative, X-band spectra were recorded in a TE$_{011}$ microwave cavity using 50 s, 100-Gauss-wide magnetic field sweeps. The instrument settings were: microwave power, 25 mW; gain, 1.0×10^4–1.0×10^6; center field, 3455–3460 Gauss; time constant, 200 ms; frequency, 9.3 GHz; and modulation, 1 Gauss at a frequency of 100 kHz. Each spectrum used in data analysis is an average of 5–20 sweeps from an individual experimental preparation. Measurements were done using kinesin·MT (kinesin bound to microtubules): kinesin in EPR-labeling buffer was added to microtubules at a stoichiometry of 1 kinesin per 5 α,β-tubulin subunits along with 5 mM ADP or AMPPNP and 5 mM MgCl$_2$. For solution measurements, this mixture was drawn into a 50-μl capillary, which was then placed in the EPR machine. For pelleted samples, the mixture was centrifuged at $70,000 \times g$ for 20 min. The supernatant was discarded, and the pellet containing microtubules and microtubule-bound kinesin molecules was scraped with a spatula onto a Rexolite flat cell. The pellet was covered with a glass coverslip, sealed with vacuum grease to prevent dehydration, and placed in the cavity. Using both methods of sample preparation, microtubule-bound samples tumble slowly enough to be completely rigid on the EPR timescale (~1000 ns), so the spectra corresponding to mobile probes reported in this work indicate that the neck linker is mobile, not that the kinesin molecules themselves are tumbling. Temperature was controlled by blowing dry air (warm or cool) into the cavity and monitored using a thermistor placed close to the experimental sample. We were able to accurately monitor the temperature to within <2°C using this technique.

Decomposition of spectral components to obtain thermodynamic data

Decomposition of spectral components was performed using a nonlinear least-squares method in which three basis spectra (one highly mobile, one intermediate, and one highly immobilized) were used to determine the proportions of these components in the composite spectra seen in our samples. This method used the fewest possible fitting parameters to obtain acceptable χ^2 values for fits, as described in this section.

The spectrum of kinesin·ADP at 35°C (see Fig. 2), which has a single, highly mobile component, was used as the ''mobile'' basis spectrum. A spectrum of kinesin·AMPPNP·MT labeled with MSL at position 333, in which virtually all of the probes are in a highly immobilized state (see Fig. 2), was obtained by taking spectra close to 0°C. Although this spectrum has no detectable mobile components, it was not simply a frozen or dried sample, because splitting between high- and low-field peaks is <72 Gauss,

TABLE 1   ATPase activity of labeled cysteine-light kinesins

Construct	k_{cat} (ATP/head/s)	K_m(MT) (μm MT)
C328-MSL	21.5 $\pm$ 1.0	1.3 $\pm$ 0.2
C330-MSL	39.7 $\pm$ 3.3	8.2 $\pm$ 1.3
C333-MSL	42.2 $\pm$ 3.7	1.9 $\pm$ 0.8
Unlabeled CLM K349	43.8 $\pm$ 2.3	4.1 $\pm$ 1.0
CLM K560 + V331A/ N332A/C333	19.1 $\pm$ 0.4	0.13 $\pm$ 0.01
Cysteine-light K560 + C333	20.2 $\pm$ 0.2	0.15 $\pm$ 0.01

ATPase assays were performed on labeled kinesin molecules (>95% of kinesins labeled) and the V331A/N332A mutant (see Methods). All labeled constructs have reasonable k_{cat} and K_m(MT) values compared to the unlabeled CLM K349 or CLMK560 + 333 construct.

which is the splitting obtained upon freezing or drying the sample. The splittings indicated for this ''immobile'' basis spectrum in Fig. 2 are ~65 Gauss, and are identical to those of the more immobilized components of kinesin·AMPPNP·MT spectra recorded at these positions at 20°C (see Fig. 1). The intermediate spectrum shown here was obtained by subtracting the mobile and highly immobilized components from a spectrum of kinesin C333-MSL·AMPPNP·MT recorded at 15°C, which contains approximately equal amounts of those two components. The residual spectrum left from this process is the intermediate spectrum used for these spectral decompositions. A difference spectrum of kinesin C333-MSL·AMPPNP·MT at 15°C (which therefore had a nonzero residual error) was used in the data analysis presented here.

Spectra were fit by a program in which χ^2 was minimized as the proportions of the three basis spectra were varied to optimize the fit. Errors in χ^2 were 0.3–2% for all spectral decompositions, which indicates that fits to three components were statistically significant. This was not the case in attempts to fit spectra to two components, which resulted in significantly higher χ^2 errors of up to 7%, even when the two components were allowed to shift laterally relative to one another as part of the fitting process. Therefore, the set of three basis spectra used here give a better fit to the data with three free parameters (the relative amounts of each of the spectra) than a set of two basis spectra give with four free parameters (the relative amounts and the relative positions of each of the spectra).

In this study, we use the same three spectra as the basis set at all temperatures and obtain very good χ^2 values (<2%) at all temperatures. This is consistent with the probe motions described by restricted motion with the motion being in the rapid limit (with correlation times <1 ns) in all components at all temperatures, and with the only variable being the amplitude of motions (order parameter). If each conformational state is characterized by a temperature-independent order parameter, then the basis spectra would be expected to be essentially independent of temperature. After decomposition of EPR spectral components, the fractions of mobile, intermediate, and immobilized probes present in each spectrum were calculated. EPR spectra as shown in Figs. 1 and 2 are ''derivative spectra,'' that is, they are plots of dA/dH versus H, where A is the absorbance of microwave energy by the sample, and H is the magnetic field. An integrated EPR spectrum would show the absorbance of microwave energy by EPR probes versus magnetic field, and the double integral of the spectrum is proportional to the total number of probes in the sample. Therefore, the relative amount of spin label in each component is found by double-integrating component spectra. The values for ΔG presented here are calculated by using the equation $\Delta G = RT \ln K$, where K is the ratio of (mobile + intermediate probes)/immobilized probes. For the purposes of this work, this is the most meaningful way of presenting the free-energy changes from the three component spectra. The mobile component reflects a free or unbound state of the kinesin neck linker, whereas the intermediate component may reflect a partially or weakly docked neck linker. Grouping these two components therefore describes all transitions from more mobile neck-linker states to the most immobilized, or completely docked, state of the kinesin neck linker. Grouping the components differently (i.e., with K as the ratio of mobile probes/(intermediate + immobilized probes)) shifts all of the absolute values for ΔG somewhat without changing the conclusions made here based on the relative values for ΔG for EPR probes at different locations in the neck linker (not shown). Enthalpies were calculated by creating Van't Hoff plots of the data ($-R \ln K$ versus $1/T$) using a linear least-squares fit. Entropies were calculated from the enthalpies and free-energy changes using the relation $\Delta G = \Delta H - T\Delta S$. More details of the data-analysis algorithm will be published elsewhere (Sindelar et al., 2002), where the same algorithm was used to calculate these thermodynamic parameters for kinesin molecules in solution. Sindelar et al. found that under certain solution conditions in the absence of microtubules, the kinesin neck linker adopts a conformation with the highly immobilized EPR spectral component seen here in microtubule-bound studies. Under these same solution conditions, kinesin crystallizes with its neck linker docked.

Decomposition of composite spectra: possible errors and implications

The thermodynamic analysis presented here requires a decomposition of the components of composite EPR spectra. The decomposition algorithm gives a residual to the fit that takes into account errors from possible components of spectra other than the three components that we consider, as well as errors due to noise in the spectra. However, this algorithm cannot take into account error induced by the possibility that the basis spectra used as pure components for spectral decompositions (see Fig. 2) may not actually be pure components, which could induce systematic error in our results. This error is likely to be fairly minimal, however, because we can resolve shifts in spectral components of a few percent, and there are undetectable amounts of the other two components in any one basis spectrum. Furthermore, because we use the same set of basis spectra (see Fig. 2) for all samples at all locations along the neck linker and all temperatures, any systematic errors introduced in the selection will contribute to all spectra and will not greatly change our calculation of ΔH values.

Evanescent field microscopy

Single kinesin-green fluorescent protein (GFP) dimers moving on Cy-5 labeled sea urchin sperm axonemes were observed under a custom-built, total internal reflection fluorescence microscope. The experiments were performed essentially the same as those by Pierce and Vale (1998), except for the
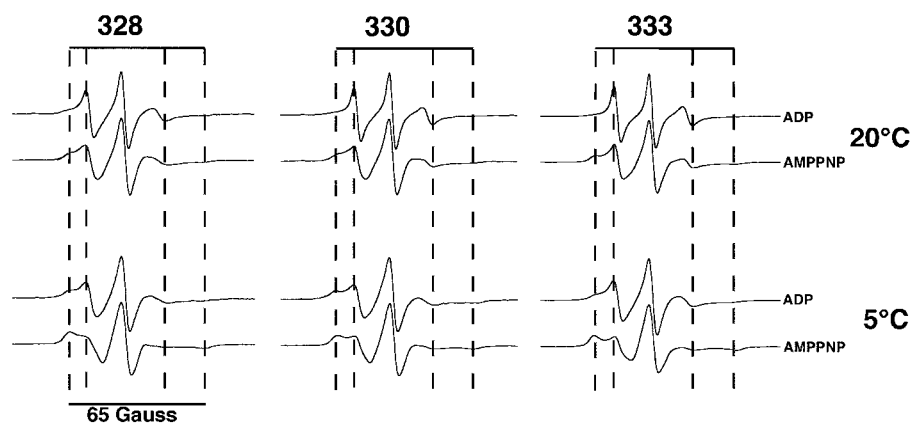

FIGURE 1 AMPPNP and ADP EPR spectra for C328, C330, and C333·MSL bound to microtubules at 20° and 5°C. Spectra were collected as described in Methods. Spectra are shown for all three positions both for kinesin·ADP·MT (*top traces*) and kinesin·AMPPNP·MT (*bottom traces*). The AMPPNP data shows a much larger immobilized component than the ADP data, as was previously reported (Rice et al., 1999). Splittings for the immobilized components are indicated as dashed lines on the spectra and are very similar for spectra recorded at all three locations. Spectra at 5°C (*bottom*) indicate that there is a significant shift of both the ADP and AMPPNP spectra to a more immobilized component at low temperature. Scale bar indicates a splitting of 65 Gauss.

Basis Spectra

Mobile   Intermediate   Immobile

65 Gauss

Spectral Decompositions

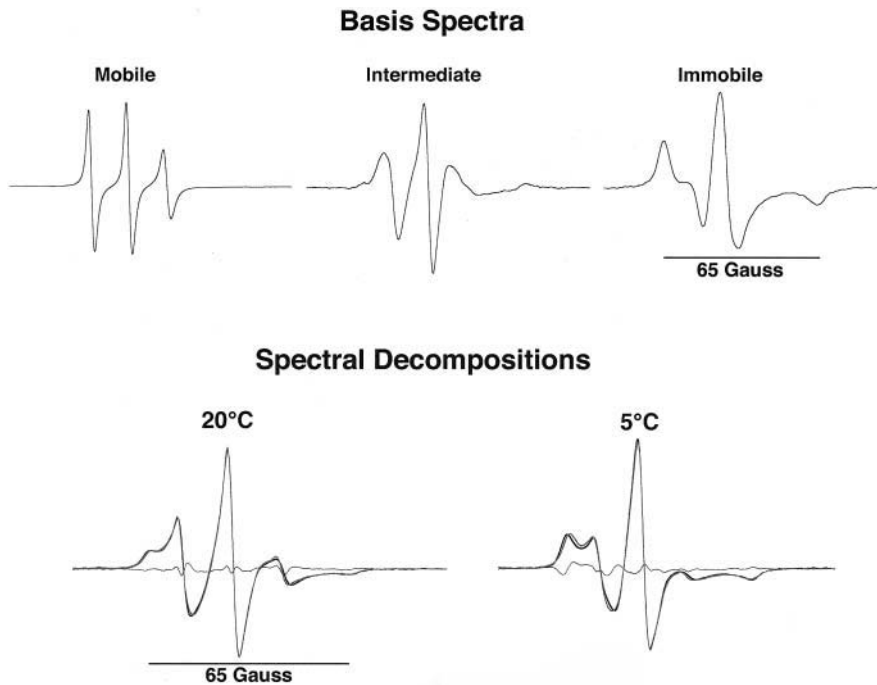20°C   5°C

65 Gauss

FIGURE 2   Mobile, intermediate, and immobilized basis spectra and sample decomposition of a composite spectrum. The mobile, intermediate, and immobilized basis spectra used to analyze all EPR data (*top*) are shown. (See Methods for details.) Example decompositions of C333·MSL·AMPPNP are shown at 20° and 5°C; actual EPR spectrum (*dark tracings*) and the fit to the basis spectra (*light tracings*) are indicated. The residual error to these fits (*light tracing near the center line*) is small for both temperatures. Similar residuals were obtained in the decompositions of other EPR spectra recorded in this study as well. The scale bars below the immobilized basis spectrum (*top right*) and the high-temperature deconvolution (*bottom left*) indicate 65 Gauss.

substitution of 7.5 mg/ml bovine serum albumin with 0.5 mg/ml casein. Kinesin-GFP motors (1–8 nM) were added to BRB12 buffer (12 mM PIPES, 2 mM MgCl$_2$, 1 mM EGTA, pH 6.8) with 1 mM ATP, casein, and oxygen scavengers. Low ionic strength (12 mM PIPES instead of 80 mM) was used in this assay, because ionic strength affects the landing rate of motors on the axoneme but does not affect the speed or run length of the motor once it attaches, which are the parameters measured here. At low ionic strength, more events are observed per experiment in the evanescent field microscope. The field was illuminated by a 5-mW argon laser beam at 488 nm, and the fluorescence images of both axonemes and GFP were averaged over four frames and recorded on an sVHS tape. The tape was then digitized at the rate of 10 frames/s and analyzed using NIH Image software with a custom-written macro. The velocity and run length of individual dimers were determined as by Romberg et al.(1998) and Shimizu et al. (2000). Velocities were fitted with a Gaussian distribution. Run lengths were determined by nonlinear least-squares fitting of the cumulative probability distribution from x_0 to infinity to $1 - \exp[(x_0 - x)/r]$ (Shimizu et al., 2000). The lower threshold, x_0, was used to exclude molecules with a run length <0.2 μm, because the measurements were inaccurate (Romberg et al., 1998), and GFP photo-bleaching was corrected for in run-length measurements as by Romberg et al. (1998).

Optical trapping experiments

The experimental procedures are essentially the same as those described by Coppin et al. (1997). Kinesin-GFP dimers were connected to 1-μm polystyrene beads through covalently coupled GFP antibodies (Tomishige and Vale, 2000). Motors were diluted to a point where approximately half of the beads exhibited movement when kept in contact with axonemes for ~1 min, so that 98% of the peaks are from a single motor (Svoboda and Block, 1994). Beads were assayed in BRB80 buffer (80 mM PIPES instead of 12 mM) with 1 mM ATP, 1 mg/ml casein, and oxygen scavengers. The data were recorded at 2 kHz and the trap stiffness (0.02–0.04 pN/nm) was calculated from the variance of the trapped bead (5 kHz) using the equipartition theorem. Data analysis was the same as described by Thorn et al. (2000). The force versus velocity curves in this work show a lower bound for

the velocity of kinesin at a given force, because the velocity is calculated making the assumption that if a motor stalls at a given force, it will also stall at larger forces (Coppin et al., 1997).

RESULTS

EPR probes placed in the kinesin neck linker undergo a large nucleotide-dependent spectral change

Our previous work used EPR spectra of probes on the neck linker of kinesin·AMPPNP·MT and kinesin·ADP·MT to reveal that the neck linker undergoes a significant conformational change (Rice et al., 1999). The change was dependent on the binding of both nucleotides and microtubules. The strength of using EPR spectroscopy to resolve these conformational changes is that, unlike most other spectroscopic techniques, EPR can resolve different spectral components that arise from distinct structural conformations present in equilibrium in a given sample. If the transition between two conformational states is slower than ~1 μs, the spectra will consist of the sum of the components of the two states. We now describe a more detailed study of the conformational changes of the neck linker, in which we perform a decomposition analysis on EPR spectral components to obtain the ΔG value for AMPPNP-induced neck-linker docking. We then use the temperature dependence of these EPR spectral components to determine the ΔH and $T\Delta S$ values for neck-linker docking. In addition, we explore the effects of mutations that are designed to alter this conformational transition.

Fig. 1 shows EPR spectra of kinesin·AMPPNP·MT and kinesin·ADP·MT labeled at positions 328, 330, or 333 with MSL at 20° and 5°C. The spectra of kinesin·MT labeled with MSL indicate a high degree of probe mobility at all three positions in the ADP state at 20°C, as described previously (Rice et al., 1999). Samples were pelleted before data collection for the spectra shown in Fig. 1 (see Methods), thereby ensuring that in both of these nucleotide states, all kinesin present was microtubule bound. Spectra recorded on samples in solution in the presence of AMPPNP are identical to the pellet spectra (not shown), which indicates that the process of pelleting the sample does not restrict probe motion. Kinesin·AMPPNP·MT spectra at all three locations at 20°C undergo a shift to a more immobilized component with very similar high-field splittings for each of the three locations indicated by the outer dashed lines in Fig. 1. The width of the splittings (distance between dashed lines in Fig. 1) reflects the degree of immobilization of the probe, which depends on interactions of the probe with the protein. Similar changes are seen in the EPR spectra of spin labels at all three of these locations along the neck linker, which indicates that a large, concerted, nucleotide-dependent conformational change occurs in this region.

EPR spectra of spin-labeled neck-linker residues show that the conformation of the neck linker depends heavily on the temperature of the sample as well as the nucleotide state. Fig. 1 shows that at 5°C, all spectra have undergone a significant shift to a more immobilized component, and the AMPPNP spectra still contain a larger amount of the immobilized component than ADP spectra. There are significant temperature-dependent changes in the EPR spectra at all three locations along the kinesin neck linker, which indicates that there is a large change in enthalpy between the structural states that corresponds to the different spectral components upon transition into the more immobilized state. Therefore, the shifts seen between the more mobile and more immobilized spectral components are not simply the result of subtle changes in the interaction between spin probes and the protein surface. Rather, an extremely large conformational change of the entire neck-linker region of kinesin takes place, involving the formation and breaking of many bonds.

Our previous spectroscopy and electron-microscopy work (Rice et al., 1999) suggested that the most immobilized conformation seen in EPR spectra corresponded to the docked neck linker for the kinesin molecule that is seen in some crystal structures (Kozielski et al., 1997; Sack et al., 1997; Song et al., 2001). This observation has been supported by a separate study in which conditions were chosen such that EPR spectra of spin-labeled kinesin molecules in solution contained a large amount of the same highly immobilized spectral component seen here in kinesin·AMPPNP·MT spectra (Sindelar et al., 2002). In a crystal structure obtained in these conditions, the kinesin neck linker is docked onto the catalytic core, as has been postulated for kinesin·AMPPNP bound to microtubules.

This is good evidence that the most highly immobilized spectral component seen in our EPR spectra is indeed the docked state of the kinesin neck linker, in which it is structured and has significant contacts with the catalytic core along its length. An intermediate component of the EPR spectrum (discussed in the following section and in Methods) may correspond to a partially docked conformation, and two steps in the docking transition have been observed using fluorescence (Rosenfeld et al., 2001).

EPR spectra can be separated into three components corresponding to different structural states

The shift to the immobilized spectral component that is seen in kinesin·AMPPNP·MT spectra relative to kinesin·ADP·MT spectra at 20°C indicates a population of probes that are in a more immobilized state, corresponding to the docked state of the kinesin neck linker. By determining the relative proportions of spin labels in each component of these EPR spectra, the changes in free energy and enthalpy for conformational changes between these states can be determined. Decomposition of EPR spectral components was performed using nonlinear least-squares fits with a basis set of three spectra obtained in part from conditions in which only one component was present. For example, the spectrum of kinesin·AMPPNP·MT at low temperatures consisted almost entirely of the immobilized spectral component. The process of spectral decomposition is described in detail (see Methods).

At the bottom of Fig. 2, the fits to the spectra of C333·MSL·MT in the presence of AMPPNP are shown at 20° and 5°C. The residual error in both of these fits is small, indicating that the same spectral components can fit these measurements at both temperatures. The same three components fit the spectral data at all three locations along the neck linker in both AMPPNP and ADP at temperatures ranging from 20° to 5°C (Fig. 1), which enabled the use of the same set of basis spectra for spectral decompositions at all three locations. This made direct cross-comparisons between probes at different locations and in different nucleotide states possible. It is possible that spectral changes observed in AMPPNP and ADP reflect entirely different conformational changes of the neck linker. The same set of basis spectra can be used to describe spectral shifts in both AMPPNP and ADP; therefore, the chemical environments of the various conformations that the probes can adopt are similar in both nucleotide states. However, this does not prove definitively that the AMPPNP and ADP docked states are identical. After decomposition of composite EPR spectra, the fractions of mobile, intermediate, and immobilized probes were calculated by double-integrating the component spectra to get the total amount of spin label in each component. These quantities were then used to calculate ΔG for conformational transitions (see Methods).

Changes in free energy associated with the neck linker conformational change are small, whereas changes in enthalpy and entropy are large

Because the different spectral components corresponding to the mobile and docked structural states of the kinesin neck linker are clearly visible in the C333·MSL·MT spectrum in the presence of AMPPNP at 20°C (Fig. 2), the ΔG between them is expected to be small. Table 2 contains values for ΔG at 20°C for MSL at positions 328, 330, and 333 in the presence of ADP and AMPPNP on microtubules, which range between -2.6 kJ/mol and -1.1 kJ/mol. The docked conformation (corresponding to the immobilized spectral component) is more favored at all three positions for kinesin·AMPPNP·MT than for kinesin·ADP·MT. The difference in free energy induced by nucleotide exchange ($\Delta\Delta G$) between the ADP and AMPPNP states indicates that the change in free energy at 20°C for the AMPPNP-induced neck-linker docking is favorable but small (~ -3 kJ/mol).

When the temperature was lowered from $\sim 20°$ to $5°C$, the EPR spectra at all three locations revealed a shift from the mobile and intermediate components to the immobile component (shown at 20° and 5°C in Fig. 1). We used spectral decompositions of the mobile, intermediate, and immobilized components of all of these spectra to quantify the temperature dependence of ΔG, which gives the enthalpy change for this conformational change. Values of ΔH for docking the neck linker in the presence of both AMPPNP and ADP were calculated at all three locations using the Van't Hoff plot of $-RlnK$ versus $1/T$, where K is the fraction of mobile and intermediate/immobilized probes and T is the temperature in Kelvin (Fig. 3; Table 2). Notably, at all three

FIGURE 3 Van't Hoff plots of C328, C330, and C333·MSL and C333·MSL/V331A/N332A in the presence of AMPPNP and ADP. Van't Hoff plots were constructed from the data (see Methods and Results). For each amino acid position, the ADP data (*solid lines*) and AMPPNP data (*dashed lines*) are shown. The linear fits for each data set used to determine the ΔH (see Table 1) were calculated using a linear least-squares method. (*A*) Van't Hoff plots for C328, C330, and C333 in the presence of both AMPPNP and ADP. (*B*) Van't Hoff plot of V331A/N332A + C333 is compared to that of C333.

sites and regardless of the nucleotide state, all changes in enthalpy are extremely large (-50 kJ/mol, on average) and within $\sim 30\%$ of each other (Fig. 3 *A*; Table 2). Corresponding to these large, favorable changes in enthalpy, there are large and unfavorable changes in entropy that result in a very small net ΔG.

A conservative neck-linker mutation causes defects in force generation

To further explore the mechanism for docking of the kinesin neck linker, we created a mutation in the neck linker that might be expected to disrupt the neck-linker-core interface

TABLE 2 Thermodynamic quantities for C328, C330, and C333-MSL and the neck-linker mutant V331A/N332A

Construct	Nucleotide	ΔG, 20°C (kJ/mol)	ΔH (kJ/mol)	$T\Delta S$ (kJ/mol)
C328	ADP	0.92	−42.9	43.8
	AMPPNP	−0.7	−50.4	49.7
C330	ADP	1.2	−54.5	55.7
	AMPPNP	−1	−40.3	39.3
C333	ADP	2.6	−51.1	53.7
	AMPPNP	−1.1	−57.5	56.4
V/N + C333	ADP	4	−59	63
	AMPPNP	2.2	−41.1	43.3

Thermodynamic parameters measured from the Van't Hoff plots of kinesin labeled with MSL at positions 328, 330, and 333, as well as the V331 A/N332A mutant labeled with MSL at position 333 are summarized. Temperature-dependent EPR spectra were recorded, and the spectral decompositions of mobile, intermediate, and immobilized components were performed (see Methods). Van't Hoff plots were fit by a least-squares method to a straight line, the slope of which is ΔH. Values of $T\Delta S$ were calculated using the ΔG and ΔH shown here. Values for ΔG at 20°C shown here were calculated using the linear fit of $-RlnK$ versus $1/T$ for all EPR spectra. This value was always very close to the ΔG at 20°C from the actual data, but it may be slightly more accurate because small errors in fitting single data sets are averaged out in the Van't Hoff plots.
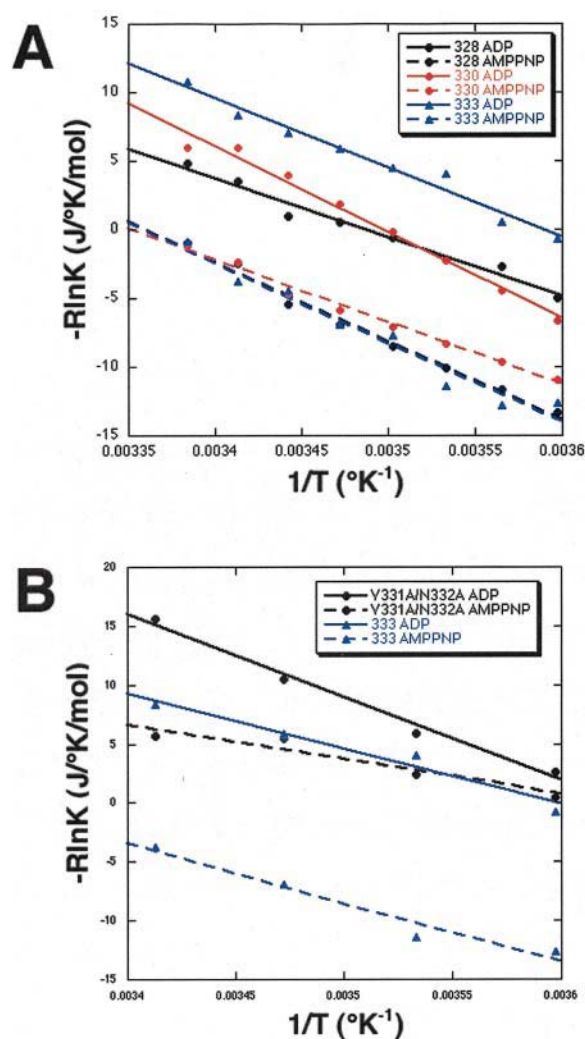
and thereby perturb the balance of ΔG, ΔH, and $T\Delta S$. This mutant, V331A/N332A, was created in the CLM K349 + C333 construct for EPR spectroscopy and in the CLM K560 + C333 construct for ATPase activity assays, force measurements, and motility measurements. We then compared the defects in the motile properties of V331A/N332A kinesin with the changes in the thermodynamic properties of its neck-linker docking. Severe mutations in the neck linker (I325A/K326A/N327A or replacement with a random 12-amino acid sequence) and in the neck-linker–catalytic core interface (G291A/G292A) have been previously reported to cause a drastic decrease in the velocity of kinesin while having little effect on its ATPase activity (Case et al., 2000). The ATPase activity of the V331A/N332A mutant (summarized in Methods) is identical to that of the CLM construct, within experimental error. Its motile characteristics, which are described in the next paragraph, show that it exhibits a significant motility defect, although this defect is far less severe than the phenotype previously described for mutants in this region of kinesin (Case et al., 2000).

Although its ATPase activity is normal, the V331A/N332A mutant has significant defects in motility and force production. The unloaded velocity of V331A/N332A (19.0 ± 9 μm/min) is significantly slower than the velocity of CLM (28.7 ± 8 μm/min). The force-velocity curve for V331A/N332A (Fig. 4 *A*) shows that this mutant is also compromised in its ability to move against an applied load. The V331/N332 mutant moves at a maximum velocity under load of 150 nm/s (~60% of CLM) and moves under a maximum force of 3 pN (~75% of CLM) in optical trapping assays. V331A/N332A also has a shorter processive run length relative to CLM kinesin (0.44 ± 0.6 μm, roughly 70% of the CLM run length). In contrast, the dissociation rate versus load characteristics of V331A/N332A are normal at loads up to its maximum 3 pN (not shown) and its K_m(MT)

is normal, which indicates that the defects seen in this mutant are not the result of weakened interaction with the microtubule. Rather, these results are consistent with a defect in the ATP-dependent neck-linker docking step, which would adversely affect the motile properties of kinesin yet have little or no effect on its ability to bind microtubules, because the motor undergoes a significant percentage of futile cycles or stalling, particularly under high loads.

Neck-linker docking is not favorable in the V331A/N332A mutant

Aside from causing defects in force generation and processivity, the V331A/N332A mutation in the kinesin neck linker disrupts the balance of thermodynamic parameters that lead to a favorable ΔG for neck-linker docking in AMPPNP. Fig. 3 *B* compares Van't Hoff plots for V331A/N332A/C333-MSL with those obtained for C333-MSL. Although the changes in enthalpy and entropy measured for these mutants are still large, they do not balance to yield a favorable ΔG for docking the neck linker in AMPPNP as for C333-MSL. For V331A/N332A, the enthalpic gain for docking in the AMPPNP state is significantly decreased relative to the CLM + C333-MSL construct. The resulting difference in the ΔG for AMPPNP-induced neck-linker docking in this mutant versus C333-MSL is substantial (Table 2), and demonstrates that although the magnitude of the favorable ΔG for neck-linker docking is small, this transition is important for the forward motility of kinesin.

DISCUSSION

Our present work indicates that the kinesin neck linker undergoes a transition between a high-entropy, disordered state and a lower-entropy, docked conformation that is sta-
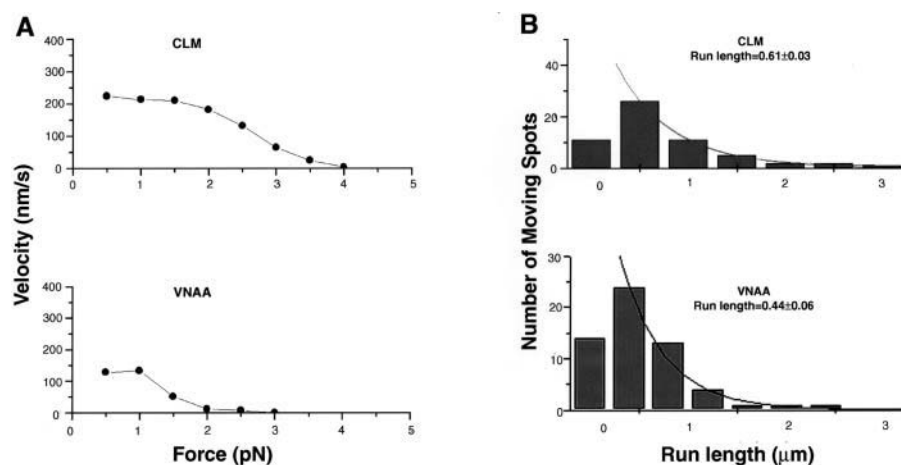

FIGURE 4 The neck-linker mutation V331A/N332A disrupts the ability of kinesin to move under large loads. (*A*) Optical trapping experiments were performed under a fixed load. The force-velocity plots shown represent a lower bound for the velocity of kinesin under load according to published data-analysis methods (Thorn et al., 2000). The V331A/N332A mutant has a significant force-production defect, but its dissociation rate under load is similar to the CLM for loads up to its stall load (data not shown). (*B*) Run-length distributions from evanescent field microscope data show that V331A/N332A has a run length that is ~70% of wild-type kinesin. Because the evanescent field microscope assay selects for spots that are moving well, the data shown here may represent an upper limit for the run lengths of this construct. The unloaded velocities, performed in the evanescent field microscope, were: CLM, 28.7 ± 8 μm/min; V331A/N332A, 19.0 ± 9 μm/min.

bilized by an increase in enthalpy. The balance between the favorable ΔH and unfavorable $T\Delta S$ for this transition results in an overall small but favorable ΔG for neck-linker docking in triphosphate states. As we expected, a mutation in the neck linker that causes motility defects also affects the thermodynamic equilibrium between free and docked states of the neck linker. These data provide new insight into the nature of the chemomechanical cycle of kinesin.

The neck linker folds onto the catalytic core

The magnitudes of the changes in entropy and enthalpy observed for the transition from the undocked to the docked state of the kinesin neck linker are consistent with the neck linker folding onto the catalytic core from a disordered state. The kinesin neck linker undergoes a change in entropy of $\sim$20 J/mol/residue, whereas a peptide binding to an antibody undergoes a change of $\sim$13 J/mol/residue (van den Elsen, 1997) and folding proteins undergo changes in entropy of 12.5–42 J/mol/residue (Creighton, 1993). Therefore, the change in entropy associated with the neck-linker conformational change is within the range observed for folding small proteins or docking short polypeptides to proteins.

In general, protein-folding transitions and short polypeptide-protein binding interactions are enthalpically driven; that is, the entropic penalty for folding a protein or docking a short polypeptide to a protein is balanced out by a substantial gain in enthalpy (Creighton, 1993; van den Elsen, 1997). Our results show that, like a protein-folding transition, the kinesin neck-linker conformational change is enthalpically driven. This is not true of all protein conformational changes or of the docking of one protein to another, which can be driven either enthalpically or entropically (Creighton, 1993). This is further evidence that the kinesin neck-linker conformational change is very similar to a protein-folding transition.

Mutations in the neck linker alter both energetics and motility

A mutation (V331A/N332A) was introduced in the neck linker to explore how the thermodynamic parameters ΔG, ΔH, and $T\Delta S$ associated with neck-linker docking relate to normal, processive kinesin motility. Neck-linker mutations in general disrupt contacts between the neck linker and the catalytic core as seen in crystal structures (Kozielski et al., 1997; Sack et al., 1997; Song et al., 2001). The most extensive hydrophobic contacts are formed in the upper region of the neck linker near I325A/K326A/N327A, and the greatest structural changes are found in this region between the disordered structure and the docked structure (Kozielski et al., 1997; Kull et al., 1996; Vale and Milligan, 2000). This is consistent with the severity of the defects seen in the neck-linker mutants created by Case et al. (2000) compared to the relatively mild phenotype of the V331A/N332A mutant described here.

The V331A/N332A mutant exhibits altered ΔH and $T\Delta S$, which is as expected for altered neck linker binding to the core. This perturbation in the thermodynamic balance between ΔH and $T\Delta S$ results in a change from the slightly favorable ΔG observed for AMPPNP-induced neck-linker docking in CLM kinesin to the unfavorable ΔG observed for this mutant.

Although the changes in both the thermodynamics of neck-linker docking and the motility of these mutants were fairly modest, they are consistent. The CLM motor generated a maximum of $\sim$4 pN of force, whereas the mutant generated $\sim$3 pN. If the docking of the neck linker produces a substep of $\sim$4 nm as found by Schnitzer et al. (2000), the difference in the work that can be performed by the mutant relative to the CLM motor is $\sim$4 pN·nm or 4 kJ/mol. This is consistent with the thermodynamic measurements from EPR spectra, which show that the ΔG for neck-linker docking in the V331A/N332A mutant is 3.3 kJ/mol less favorable ($+$2.2 kJ/mol) than the CLM ($-$1.1 kJ/mol). Although neck-linker docking is always unfavorable at 20°C for this mutant, the docking transition still occurs, and the motor is still able to move because the subsequent step, which involves the binding of a kinesin head to the microtubule, is very favorable.

A small, favorable ΔG efficiently generates the forward bias of kinesin

The data presented here indicate that there is a small, favorable ΔG for the AMPPNP-induced neck-linker docking that creates the forward bias of kinesin. This supports the idea that in the course of a single enzymatic cycle and coupled mechanical advance, kinesin undergoes an ATP-dependent isomerization step with a small change in free energy before undergoing an ATP-independent step with a large change in free energy (Schnitzer et al., 2000). Our measurements lead to the conclusion that the ATP-dependent isomerization is the neck-linker docking to the catalytic core (Rice et al., 1999), and the ATP-independent step is the second kinesin head binding to the microtubule.

Despite the small magnitude of the free-energy change for AMPPNP-induced docking of the kinesin neck linker, it is critical to the forward motility of kinesin. A balance between the favorable enthalpy and entropy changes from burying hydrophobic residues in the neck-linker–core interface and the unfavorable entropy change from docking the kinesin neck linker shifts upon AMPPNP binding, causing the docked state to become energetically favorable. This may occur because conformational changes in the neck-core interface allow for energetically beneficial contacts to be formed between the neck linker and the catalytic core, which offset the high entropic cost for folding the neck linker along the core.

Our conclusions are that a very small free-energy change leads to the forward bias and efficient motility of kinesin. This seemingly contradicts the finding that kinesin very rarely takes backward steps. We present here a simple illustration of

how a motor can move predominantly unidirectionally with very high efficiency while using only a small amount of its available free energy from ATP to create a forward bias.

Assume that a linear motor can move in either direction along a track, hydrolyzing one ATP per step. Further, assume that the motor uses a portion of the free energy gained from ATP to generate a forward bias and the rest to do work by stepping against a load in whichever direction it steps. This simple model can be described by the following equations:

$$\Delta G_{ATP} = \Delta G_{bias} + \Delta G_{work}$$

$$\Delta G_{bias} = -RT \times \ln(\text{forward steps}/\text{backward steps})$$

$$\text{Efficiency forward} \propto (\text{no. of forward steps} \times \Delta G_{work} \\ - \text{no. of backward steps} \times \Delta G_{work}).$$

If the motor devotes no energy toward creating a forward bias, it does the maximum amount of work per step, but steps in both directions equally, resulting in no net forward motion. If the motor puts most of its ATP into creating a bias, it always moves in one direction but generates less work per step. By solving the equations, one finds that the motor operates at maximal efficiency between these two extremes, where it uses 18% of its available free energy from ATP hydrolysis to generate a unidirectional bias and the rest to do work. Although this model is highly qualitative, it illustrates a major point: because the ratio of forward to backward steps depends exponentially on ΔG_{bias}, the motor does not have to spend much free energy on its bias to move almost completely unidirectionally forward. Furthermore, in motility assays, this maximum-efficiency motor would be expected to take ~12% backsteps, comparable to the 10% seen for kinesin operating at high force (maximum efficiency) (Visscher et al., 1999).

The highly disordered state of the undocked neck linker can play a role in the unidirectional, processive movement of kinesin

The processive, unidirectional motion of a kinesin dimer along a microtubule requires the coordination of the sequential binding and release of the two heads from the microtubule. Here we discuss the possibility that the unstructured conformation of the undocked neck linker plays a central role in this coordination by producing the preferential detachment of the trailing head and preventing it from rebinding to the microtubule behind the leading head. As we argued previously, the docking of the neck linker upon binding of ATP to a microtubule-bound motor domain moves the unattached head of the dimeric molecule toward the

A.
Rear neck linker is docked
Front neck linker is held in a low entropy state

B.
Pi and MT release by rear head,
Entropic collapse of neck linkers brings rear head forward and prevents backward stepping

C.
ATP induces Neck linker docking by rear head
Small ΔG
Large ΔH, TΔS

D.
Front head binds MT
Large ΔG of binding
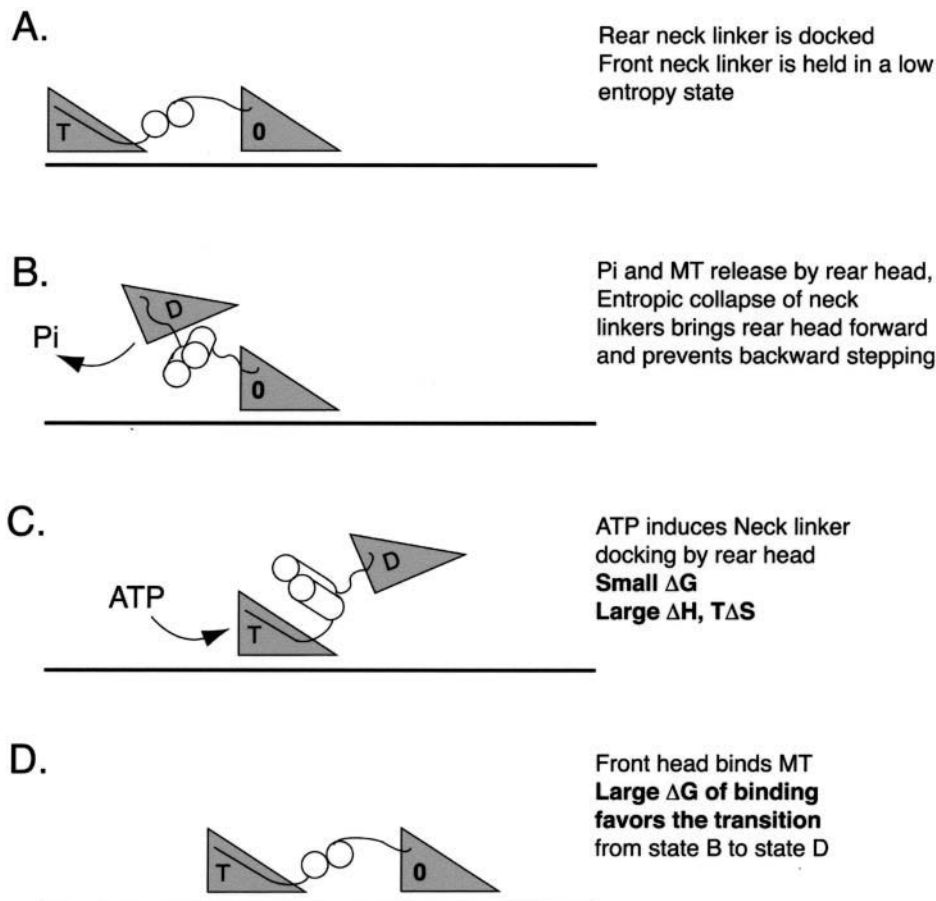favors the transition from state B to state D

FIGURE 5   A model for a folding transition in the kinesin neck linker. This model shows how the transition of the neck linkers of a kinesin dimer into a high-entropy state may affect the motility of kinesin. (*A*) The trailing head is bound to the microtubule (MT) with its neck linker docked along its catalytic core, the leading head bound with its nucleotide site empty (marked with a ''0''), and its neck linker held in an entropically strained conformation. (*B*) When the trailing head releases phosphate, its neck linker dissociates from its catalytic core, and the trailing head dissociates from the microtubule. The entropic strain of the two neck linkers creates a force pulling the trailing head forward and preventing it from rebinding behind the leading head. (*C*) Binding of ATP to the head that is bound to the MT docks its neck linker along the catalytic core, throwing the second head in front of it. (*D*) The unbound head then binds tightly to the MT in front of the other head. The large ΔG of binding to the MT makes the transition from *C* to *D* favorable despite the small value for the ΔG of docking of the neck linker.

microtubule plus end. When the unattached head binds the microtubule in front of the attached head, its neck linker is undocked while that of the trailing head is docked (Fig. 5 *A*). At this point in the cycle, the trailing head hydrolyzes ATP, releases phosphate, its neck linker detaches from the catalytic core, and the head detaches from the microtubule (Fig. 5 *B*). In the state illustrated by Fig. 5 *B*, both neck linkers assume a random conformation, and the nature of this conformation will generate an elastic element.

The properties of random polymers such as the neck linkers of the two kinesin heads in the disordered conformation have been thoroughly investigated. The most likely configuration is one in which the polymer assumes a compact structure with an end-to-end distance given by

$$D = C \times L_0 \times N^{1/2}$$

where D is the end to end distance, L_0 is the length of the subunit of the polymer (3.8 Å for an amino acid), N is the number of subunits (~30 for two neck linkers), and C is a constant, which is ~2 for polypeptides (Miller and Goebel, 1968). This equation predicts that the equilibrium length of two disordered neck linkers would be ~50 Å, considerably shorter than the known end-to-end distance of 80 Å when both heads are bound to the microtubule. Therefore, undocking of the neck linker of the trailing head by the release of phosphate will generate a force between the two heads that is driven by the entropy gained by the two neck linkers in assuming a more compact form. Assuming a ''wormlike chain'' model for the two neck linkers, this force can be very large, on the order of 5–15 pN (Bustamante et al., 1994; Marko and Siggia, 1995). The trailing head will preferentially detach from the microtubule and be pulled forward ~30 Å by these entropic forces, which is half of the kinesin step size (Fig. 5 *B*). Alternatively, release of the trailing head from the microtubule with subsequent release of phosphate will arrive at the same state. Rebinding of the trailing head in the reverse direction from this state will be greatly hindered by the elastic element of the two undocked neck linkers.

Two factors will lead to the preferential detachment of the trailing head rather than the leading head, which yields a forward step. The trailing head has a bound ADP at this point in the cycle that produces a weaker interaction with the microtubule. In addition, the force required to detach a kinesin head from the microtubule is greater if the force is applied in the minus direction rather than in the plus direction (Uemura et al., 2002).

This model concludes that the rubberlike elastic force generated by the two disordered neck linkers produces a force-generating step in the kinesin cycle and leads to the preferential detachment of the rear head. This is supported by several experimental observations. Kinesin monomers as well as single-headed kinesin dimers are unable to adopt the strained conformation shown in Fig. 5 *A* and have a significantly slowed release rate from the microtubule (Hancock and Howard, 1998; Jiang and Hackney, 1997; Ma

and Taylor, 1997b; Moyer et al., 1998), indicating that detachment from the microtubule in the rear head may be accelerated by this strained conformation. High-resolution optical trapping data shows that the kinesin step is comprised of a fast, 4-nm substep (Nishiyama et al., 2001), which may correspond to the entropic collapse of the neck linkers (as in Fig. 5 *B*), and a subsequent slow substep, which may correspond to the docking of the bound-head neck linker and subsequent rebinding of the front head (Fig. 5, *C* and *D*). Furthermore, this model predicts very few backsteps, because backsteps would be made energetically unfavorable by the entropic collapse of the neck linkers despite the small ΔG observed for forward neck-linker docking. In several different types of assays, kinesin has been shown to take very few backward steps (Coppin et al., 1997; Coy et al., 1999; Hua et al., 1997; Schnitzer and Block, 1997; Svoboda and Block, 1994; Visscher et al., 1999). The model in Fig. 5 illustrates kinesin walking by a symmetric hand-over-hand mechanism for simplicity. Recent experiments have suggested that kinesin may not move by this type of mechanism and instead might ''inchworm'' along the microtubule or move by an asymmetric hand-over-hand mechanism (Hua et al., 2002). The elastic force generated between two unstructured neck linkers described here may be an important aspect of the motility of kinesin regardless of the exact mechanism of its motion, which has yet to be determined.

CONCLUSIONS

We have used temperature-dependent EPR spectroscopy to determine the thermodynamic properties, ΔG, ΔH, and $T\Delta S$ associated with the AMPPNP-induced docking of the kinesin neck linker that generates its forward bias and drives motility. The free-energy changes associated with the neck-linker conformational change were favorable but small (~3 kJ/mol). The large, favorable enthalpy changes balanced out by large unfavorable entropy changes indicate that the neck linker docks to the core from an unstructured state, in a conformational change that is similar to a protein-folding transition. Kinesin uses only a small portion of its free energy available from ATP to generate a forward bias, a property that may enable it to be a very efficient motor. The kinesin neck linker undocks and undergoes a transition into a high-entropy state, which suggests the possibility that entropic strain plays an important role in generating the nearly unidirectional forward motility of the kinesin dimer.

REFERENCES

Bustamante, C., J. F. Marko, E. D. Siggia, and S. Smith. 1994. Entropic elasticity of lambda-phage DNA. *Science* 265:1599–1600.

Case, R. B., D. W. Pierce, N. Hom-Booher, C. L. Hart, and R. D. Vale. 1997. The directional preference of kinesin motors is specified by an element outside of the motor catalytic domain. *Cell* 90:959–966.

Case, R. B., S. Rice, C. L. Hart, B. Ly, and R. D. Vale. 2000. Role of the kinesin neck linker and catalytic core in microtubule-based motility. *Curr. Biol.* 10:157–160.

Coppin, C. M., D. W. Pierce, L. Hsu, and R. D. Vale. 1997. The load dependence of kinesin's mechanical cycle. *Proc. Natl. Acad. Sci. USA* 94:8539–8544.

Coy, D., M. Wagenbach, and J. Howard. 1999. Kinesin takes one 8-nm step for each ATP it hydrolyzes. *J. Biol. Chem.* 274:3667–3671.

Creighton, T. E. 1993. Proteins: Structures and Molecular Properties. W. H. Freeman and Co., New York. 507 p.

Gilbert, S. P., M. L. Moyer, and K. A. Johnson. 1998. Alternating site mechanism of the kinesin ATPase. *Biochemistry* 37:792–799.

Hackney, D. D. 1994. Evidence for alternating head catalysis by kinesin during microtubule-stimulated ATP hydrolysis. *Proc. Natl. Acad. Sci. USA* 91:6865–6869.

Hancock, W. O. and J. Howard. 1998. Processivity of the motor protein kinesin requires two heads. *J. Cell Biol.* 140:1395–1405.

Henningsen, U. and M. Schliwa. 1997. Reversal in the direction of movement of a molecular motor. *Nature* 389:93–95.

Hoenger, A., S. Sack, M. Thormahlen, A. Marx, J. Muller, H. Gross, and E. Mandelkow. 1998. Image reconstructions of microtubules decorated with monomeric and dimeric kinesins: comparison with x-ray structure and implications for motility. *J. Cell Biol.* 141:419–430.

Hoenger, A., M. Thormahlen, R. Diaz-Avalos, M. Doerhoefer, K. Goldie, J. Muller, and E. Mandelkow. 2000. A new look at the microtubule binding patterns of dimeric kinesins. *J. Cell Biol.* 297:1087–1103.

Hua, W., J. Chung, and J. Gelles. 2002. Distinguishing inchworm and hand-over-hand processive kinesin movement by neck rotation measurements. *Science* 295:844–848.

Hua, W., E. C. Young, M. L. Fleming, and J. Gelles. 1997. Coupling of kinesin steps to ATP hydrolysis. *Nature* 388:390–393.

Jiang, W. and D. D. Hackney. 1997. Monomeric kinesin head domains hydrolyze multiple ATP molecules before release from a microtubule. *J. Biol. Chem.* 272:5616–5621.

Kikkawa, M., E. P. Sablin, Y. Okada, H. Yajima, R. J. Fletterick, and N. Hirokawa. 2001. Switch-based mechanism of kinesin motors. *Nature* 411:439–445.

Kozielski, F., S. Sack, A. Marx, M. Thormahlen, E. Schonbrunn, V. Biou, A. Thompson, E. M. Mandelkow, and E. Mandelkow. 1997. The crystal structure of dimeric kinesin and implications for microtubule-dependent motility. *Cell* 91:985–994.

Kull, F. J. and S. A. Endow. 2002. Kinesin: switch I and II and the motor mechanism. *J. Cell Sci.* 115:15–23.

Kull, J. F., E. P. Sablin, R. Lau, R. J. Fletterick, and R. D. Vale. 1996. Crystal structure of the kinesin motor domain reveals a structural similarity to myosin. *Nature* 380:550–555.

Ma, Y.-Z. and E. W. Taylor. 1997a. Interacting head mechanism of microtubule-kinesin ATPase. *J. Biol. Chem.* 272:724–730.

Ma, Y. Z. and E. W. Taylor. 1997b. Kinetic mechanism of a monomeric kinesin construct. *J. Biol. Chem.* 272:717–723.

Marko, J. F. and E. D. Siggia. 1995. Statistical mechanics of supercoiled DNA. *Phys. Rev. E. Stat. Phys. Plasmas Fluids Relat. Interdiscip. Topics.* 52:2912–2938.

Miller, W. and C. Goebel. 1968. Dimensions of protein random coils. *Biochemistry* 7:3925–3935.

Moyer, M. L., S. P. Gilbert, and K. A. Johnson. 1998. Pathway of ATP hydrolysis by monomeric and dimeric kinesin. *Biochemistry* 37:800–813.

Naber, N., R. Cooke, and E. Pate. 1997. Binding of ncd to microtubules induces a conformational change near the junction of the motor domain with the neck. *Biochemistry* 36:9681–9689.

Nishiyama, M., E. Muto, Y. Inoue, T. Yanagida, and H. Higuchi. 2001. Substeps within the 8-nm step of the ATPase cycle of single kinesin molecules. *Nat. Cell Biol.* 3:425–428.

Pierce, D. W. and R. D. Vale. 1998. Assaying processive movement of kinesin by fluorescence microscopy. *Meth. Enzymol.* 298:154–171.

Rice, S., A. W. Lin, D. Safer, C. L. Hart, N. Naber, B. O. Carragher, S. M. Cain, E. Pechatnikoval, E. M. Wilson-Kubalek, M. Whittaker, E. Pate, R. Cooke, E. W. Taylor, R. A. Milligan, and R. D. Vale. 1999. A structural change in the kinesin motor protein that drives motility. *Nature* 402:778–783.

Romberg, L., D. W. Pierce, and R. D. Vale. 1998. Role of the kinesin neck region in processive microtubule-based motility. *J. Cell Biol.* 140:1407–1416.

Rosenfeld, S. S., G. M. Jefferson, and P. H. King. 2001. ATP reorients the neck linker of kinesin in two sequential steps. *J. Biol. Chem.* 276:40167–40174.

Sablin, E. P. and R. J. Fletterick. 2001. Nucleotide switches in molecular motors: structural analysis of kinesins and myosins. *Curr. Opin. Struct. Biol.* 11:716–724.

Sack, S., J. Muller, A. Marx, M. Thormahlen, E. M. Mandelkow, S. T. Brady, and E. Mandelkow. 1997. X-ray structure of motor and neck domains from rat brain kinesin. *Biochemistry* 36:16155–16165.

Schnitzer, M. J. and S. M. Block. 1997. Kinesin hydrolyzes one ATP per 8-nm step. *Nature* 388:386–390.

Schnitzer, M. J., K. Visscher, and S. M. Block. 2000. Force production by single kinesin motors. *Nat. Cell Biol.* 2:718–723.

Shimizu, T., K. S. Thorn, A. Ruby, and R. D. Vale. 2000. ATPase kinetic characterization and single molecule behavior of mutant human kinesin motors defective in microtubule-based motility. *Biochemistry* 39:5265–5273.

Sindelar, C. V., M. J. Budny, S. E. Rice, N. Naber, R. Fletterick, and R. Cooke. 2002. Two conformations in the human kinesin power stroke defined by x-ray crystallography and EPR spectroscopy. *Nat. Struct. Biol.* 9:844–848.

Song, Y.-H., A. Marx, J. Muller, G. Woehlke, M. Schliwa, A. Krebs, A. Hoenger, and E. Mandelkow. 2001. Structure of a fast kinesin: implications for ATPase mechanism and interactions with microtubules. *EMBO J.* 20:6213–6225.

Svoboda, K. and S. M. Block. 1994. Force and velocity measured for single kinesin molecules. *Cell* 77:773–784.

Thomas, D. D. and R. Cooke. 1980. Orientation of spin-labeled myosin heads in glycerinated muscle fibers. *Biophys. J.* 32:891–906.

Thorn, K. S., J. A. Ubersax, and R. D. Vale. 2000. Engineering the processive run length of the kinesin motor. *J. Cell Biol.* 151:1093–1100.

Tomishige, M. and R. D. Vale. 2000. Controlling kinesin by reversible disulfide crosslinking: identifying the motility-producing conformational change. *J. Cell Biol.* 151:1081–1092.

Uemura, S., K. Kawaguchi, J. Yajima, M. Edamatsu, Y. Y. Toyoshima, and S. Ishiwata. 2002. Kinesin-microtubule binding depends on both nucleotide state and loading direction. *Proc. Natl. Acad. Sci. USA* 99:5977–5981.

Vale, R. D., T. Funatsu, D. W. Pierce, L. Romberg, Y. Harada, and T. Yanagida. 1996. Direct observation of single kinesin molecules moving along microtubules. *Nature* 380:451–453.

Vale, R. D. and R. A. Milligan. 2000. The way things move: looking under the hood of molecular motors. *Science* 288:88–95.

van den Elsen, J. M. H., L. M. van Unen, L. van Bloois, M. A. Busquets, W. Jiskoot, P. Hoogerhout, J. Wilting, J. N. Herron, and D. J. Crommelin. 1997. Thermodynamic analysis of the interaction between a bactericial antibody and a porA epitope of *Nesseria* meningitidis. *Biochemistry* 36:12583–12591.

Visscher, K., M. J. Schnitzer, and S. M. Block. 1999. Single kinesin molecules studied with a molecular force clamp. *Nature* 400:184–189.

Woehlke, G., A. K. Ruby, C. L. Hart, B. Ly, N. Hom-Booher, and R. D. Vale. 1997. Microtubule interaction site of the kinesin motor. *Cell* 90:207–216.

Yun, M., X. Zhang, C.-G. Park, H.-W. Park, and S. A. Endow. 2001. A structural pathway for activation of the kinesin motor ATPase. *EMBO J.* 20:2611–2618.